HHS Public Access

Author manuscript

Magn Reson Med. Author manuscript; available in PMC 2015 May 18.

Published in final edited form as:

Magn Reson Med. 2015 April ; 73(4): 1579–1592. doi:10.1002/mrm.25268.

Dual Echo Vessel-Encoded ASL for Simultaneous BOLD and CBF Reactivity Assessment in Patients with Ischemic Cerebrovascular Disease

Carlos C. Faraco[1,*], **Megan K. Strother**[1], **Lindsey M. Dethrage**[1], **Lori Jordan**[2], **Robert Singer**[3], **Paul F. Clemmons**[1], and **Manus J. Donahue**[1,2,4,5]

[1]Department of Radiology and Radiological Sciences, Vanderbilt University School of Medicine, Nashville, Tennessee, USA

[2]Department of Neurology, Vanderbilt University School of Medicine, Nashville, Tennessee, USA

[3]Section of Neurosurgery, Geisel School of Medicine, Dartmouth-Hitchcock Medical Center, Lebanon, New Hampshire, USA

[4]Department of Psychiatry, Vanderbilt University School of Medicine, Nashville, Tennessee, USA

[5]Department of Physics and Astronomy, Vanderbilt University, Nashville, Tennessee, USA

Abstract

Purpose—Blood oxygenation level-dependent (BOLD)-weighted and vessel-encoded arterial spin labeling (VE-ASL) MRI provide complementary information and can be used in sequence to gauge hemodynamic contributions to cerebrovascular reactivity. Here, cerebrovascular reactivity is assessed using dual echo VE-ASL MRI to understand how VE labeling preparations influence BOLD and ASL contrast in flow-limited and healthy perfusion territories.

Methods—Patients (n = 12; age = 55 +/− 14 years; 6F/6M) presenting with ischemic steno-occlusive cerebrovascular disease underwent 3.0T angiographic imaging, T_1-weighted structural, and planning-free dual echo hypercarbic hyperoxic (i.e., carbogen) VE-ASL MRI. Vasculopathy extent, timecourses, and cerebrovascular reactivity (signal change and Z-statistic) for different VE-ASL images were contrasted across flow territories and Bonferroni-corrected P-values reported.

Results—BOLD cerebrovascular reactivity (i.e., long-TE VE-ASL) Z-statistics were similarly sensitive to asymmetric disease ($P \leq 0.002$) regardless of labeling scenario. Cerebral blood flow reactivity correlated significantly with BOLD reactivity (Z-statistic). However, BOLD signal changes did not differ significantly between labeling scenarios (P>0.003) or across territories (P>0.002), indicating BOLD signal changes in response to carbogen offer low sensitivity to lateralizing disease.

*Correspondence to: Carlos Cesar Faraco, Ph.D., Vanderbilt University Institute of Imaging Science, 1161 21st Ave S, MCN, AAA-1112, Nashville, TN 37232–2310. carlos.c.faraco.1@vanderbilt.edu.

Additional Supporting Information may be found in the online version of this article.

Conclusion—Dual echo VE-ASL can provide simultaneous cerebral blood flow and qualitative BOLD contrast consistent with lateralizing disease severity in patients with asymmetric steno-occlusive disease. The methodological strengths and limitations of composite BOLD and VE-ASL measurements in the clinic are discussed.

Keywords

arterial spin labeling; blood oxygenation level dependent; vessel-encoded arterial spin labeling; cerebrovascular reactivity; hemodynamics; stroke

INTRODUCTION

Cerebral blood flow (CBF) monitoring has been shown to provide diagnostic (1–6) and prognostic (7) information in patients with cerebrovascular disease. Arterial spin labeling (ASL) MRI enables CBF measurement noninvasively (8,9) and therefore has great potential for longitudinally tracking changes in CBF in cases where exogenous contrast agents may be dose restricted or contraindicated. In conventional ASL, arterial blood water is magnetically labeled in inflowing cervical vessels using a single (2,9) or multiple (10,11) radiofrequency pulses, after which a delay time is allowed (e.g., 1.5 s–2 s) in which the labeled blood water flows into the capillary exchange site, exchanges with tissue water, and attenuates the extravascular water signal. More recently, advancements in ASL have enabled assessment of individual vessel perfusion territories through vessel-specific labeling of blood water (12–14), known as vessel-encoded ASL (VE-ASL). Simultaneous quantification of flow territories and CBF may provide further clinical potential for risk assessment and therapeutic treatment planning, yet the clinical role of VE-ASL is still in relatively early stages of investigation.

Assessment of cerebrovascular reactivity (CVR), or how near the vasculature is to exhausting reserve capacity, using ASL provides a partial indicator of vascular compliance, as the measurement primarily reflects CBF reactivity. Another common method of assessing CVR is through blood oxygenation level-dependent (BOLD) MRI, which reports on susceptibility-induced changes in and around vessels during changes in blood oxygenation. BOLD imaging, however, is also only a partial indicator of vascular compliance, as it consists of indirect contributions from CBF, cerebral blood volume (CBV), and when applicable, the cerebral metabolic rate of oxygen consumption. Nevertheless, BOLD is more frequently used to assess CVR, primarily owing to a multifold increase in signal-to-noise ratio (SNR) and improved temporal resolution (1 s–3 s) compared to ASL (4 s–8 s).

More specifically, MRI-based assessment of CVR frequently utilizes hypercarbic gas stimuli, which when administered for short durations (i.e., ≤3 min) elicit a primarily isometabolic (15–19) increase in CBF and CBV, (20–22), resulting in increased capillary and venous blood oxygenation. The magnitude of the change in oxygenation, and therefore BOLD response, provides a surrogate marker of CVR. The drawback of hypercarbia-induced BOLD CVR measurements is that the resulting BOLD response is hemodynamically nonspecific, with small contributions from R_2* changes in and around arteries (i.e., from potential changes in ventilation, arterial oxygenation, and arterial CBV)

and larger contributions from R_2* changes in and around veins (i.e., from potential changes in ventilation, venous oxygenation, and venous CBV). Therefore, it would be desirable to increase the number of observables in such experiments by performing measurements of CBF and BOLD sequentially or simultaneously.

As BOLD and ASL become more common in patient populations (1,3,23–27), the possibility of integrating these sequences into standard protocols for assessment of cerebrovascular status deserves investigation. As MRI protocol durations are often more limited in patients, it may be impractical to prescribe separate ASL and BOLD acquisitions, especially in conjunction with hypercarbic gas challenges and/or multiple VE labeling scenarios. This can be resolved by dual echo ASL, in which a short echo time (TE) provides predominately flow-weighted contrast, whereas a longer TE centered on tissue water T_2^* provides BOLD contrast (28–30). Generally, only the unlabeled long-TE images have been thought ideal for BOLD processing; however, this lowers the BOLD temporal resolution to 4–8 s (depending on spin labeling implementation). This problem is exacerbated during VE-ASL implementations where multiple labeling scenarios are interleaved with the control acquisition. Here, the temporal resolution may be 20 s or more, depending on the number of labeling conditions.

While dual echo ASL acquisitions have been investigated, no information is available on the stability of multiecho VE-ASL for simultaneous flow territory mapping, CBF reactivity, and BOLD CVR assessment. Here, we implemented a dual echo VE-ASL sequence in patients with symptomatic intracranial (IC) steno-occlusive disease with lateralizing flow-limiting stenosis quantified from independent measurements derived from digital subtraction angiography, magnetic resonance angiography, or computed tomography angiography. The overall hypothesis to be investigated is that dual echo VE-ASL is feasible in a clinical setting for simultaneous measurement of flow territories, CBF CVR, and BOLD CVR, and, provides lateralizing contrast consistent with independently confirmed vascular steno-occlusive disease. A secondary hypothesis is that in VE-ASL acquisitions that rely on constant (i.e., nonpatient-tailored) vessel labeling geometries, the small effect of the flow labeling on long-TE (i.e., BOLD weighted) CVR will not significantly confound CVR assessment. Verification of this latter hypothesis would provide evidence for the feasibility of dual echo VE-ASL for CBF and BOLD CVR assessment while maintaining moderate BOLD temporal resolution (<5 s). Finally, the strengths and limitations of this approach are discussed in the context of clinical imaging constraints in patients with cerebrovascular disease.

METHODS

Participants

Patients (n = 23; age = 50 +/− 18 years; sex = 14F/9M) presenting with symptoms consistent with ischemic cerebrovascular disease provided informed, written consent as required by the local Institutional Review Board, and were recruited through the Vanderbilt University Medical Center as part of a larger, prospective clinical trial (Vanderbilt Assessment of Multimodal Mri in Patients at Risk for stroke with Intracranial Stenosis, VAMMPRIS). Patients presented with atherosclerotic IC stenosis (n = 15), nonatherosclerotic IC stenosis

(i.e., Moyamoya disease; $n = 6$), arteriovenous malformation ($n = 1$), and craniometaphyseal dysplasia ($n = 1$). The purpose of this study was to compare BOLD and VE-ASL CVR measures in asymmetric steno-occlusive disease, therefore we applied the following inclusion criteria to select a subpopulation of participants for completion of this aim: angiographic evidence of at least unilateral IC vessel (ICA, MCA, ACA, and/or PCA segments) stenosis ≥50% as verified by a board-certified neuro-radiologist (M.K.S.; neuroradiology experience = 13 years). Patients with significant cervical (extracranial ICA or extracranial basilar artery) stenosis (≥70%) and/or bilateral (≥70%) ICA stenoses were excluded. Furthermore, patients with arterial blood oxygenation saturation ≤90% were not scanned due to possible safety concerns associated with the hypercarbia protocol.

MRI

Patients were scanned at 3.0T (Philips, Best, The Netherlands) using body coil transmission and 8-channel SENSE reception. Patients were fitted with a nasal cannula to measure end-tidal CO_2 ($EtCO_2$) levels and a nonrebreathing mask to supply medical grade room air (21% O_2, 79% N_2) or a carbogen mixture (5% CO_2, 95% O_2); other patient vitals (e.g., sPO_2, heart rate, and blood pressure) were monitored by a respiratory therapist. Carbogen administration, as opposed to 5% CO_2/balanced room air, was required as a conservative safety measure to ensure that the fraction inspired O_2 (FiO_2) would not decrease, which could exacerbate stroke risk in subacute patients. Confounds resulting from this hypercarbic hyperoxic challenge are worthwhile to note and are summarized in the Discussion.

Patients underwent a multimodal imaging protocol consisting of the following scans: (i) T_1-weighted (MPRAGE: $1 \times 1 \times 1$ mm^3; TR/TE = 8.9/4.6 ms; duration = 3 min 47 s), (ii) T2-weighted FLAIR ($0.9 \times 0.9 \times 1$ mm^3 ; TR/TE = 11,000/120 ms; multishot turbo spin echo inversion recovery; duration = 1 min 39 s), and (iii) hypercarbic dual echo CBF-weighted pseudo-continuous ASL (pCASL); $3.5 \times 3.5 \times 7$ mm^3 ; TR/TE1/TE2/PLD: 4500/10.5/35/1600 ms; 17 slices; ascending acquisition; 1500 ms Hanning labeling pulse train; 90 mm labeling offset; duration = 15 min). VE-ASL labeling was performed to assess flow territories corresponding to the left ICA (L ICA), right ICA (R ICA), and vertebrobasilar arteries (VBAs). For each patient, flow territory mapping was achieved using a previously reported automated procedure (31,32) with five labeling scenarios: (i) no label (control), (ii) nonspecific labeling of all inflowing vessels (full label), (iii) varying inversion efficiency by 9 mm in A/P direction (VBA1 labeling), (iv) 9 mm in A/P shifted by 4.5 mm (VBA2 labeling), and (v) 25 mm in R/L direction (R ICA labeling). The labeling conditions are shown schematically in Figure 1. A block paradigm consisting of alternating 3 min blocks of breathing room air or carbogen was used during the dual echo VE-ASL acquisition, resulting in three blocks of room air inhalation and two blocks of carbogen inhalation.

Digital Subtraction Angiography/Magnetic Resonance Angiography/Computed Tomography Angiography

Location and degree of vessel stenosis was determined from clinical angiographic imaging data. Briefly, fourvessel digital subtraction angiography was performed in the neuroangiography suite using a Philips Allura Xper biplane neuro X-ray system with the

patient in the supine position. Selected arterial catheterizations of bilateral ICAs and bilateral vertebral arteries were performed in multiple projections using nonionic, watersoluble intra-arterial contrast. All injections were performed by hand by the collaborating vascular surgeon using the following volumes and rates: ICA injections— 3–4 cc over 0.5 s, external carotid artery (ECA) injections— 2–3 cc over 2 s, common carotid artery (CCA) injections—4–5 cc over 0.5 s. Digital images were acquired at three frames/s for the first 4 s, then one frame/s for the next 8 s, and 0.5 frames/s thereafter. Stenosis degree was classified as the ratio of the width of the stenosed lumen to the width of the normal distal vessel. If there was no normal distal vessel, the stenosed lumen was measured against the normal lumen proximal to the stenosis. All angiography was performed within 60 days of the VE-ASL experiment.

Angiographic images were also used to grade posterior communicating artery (PCOM) status into three categories. These were (1) fetal PCOM, where the PCOM was present and no ipsilateral P1 was identified, (2) fetaltype PCOM, where the PCOM was present and larger than the ipsilateral P1, and (3) PCOM present, where the PCOM was present and smaller than the ipsilateral P1.

BOLD Analysis

MRI data were analyzed using in-house Matlab (Mathworks, Natick, MA) code and routines available from the FMRIB software library, FSL (33,34). First, affine motion correction, linear slice-time correction, and spatial smoothing (FWHM = 6 mm with Gaussian kernel) were applied. Baseline drift correction was performed on a voxel-wise basis by quadratic polynomial regression (35). Subsequently, functional data were coregistered to a standard atlas (Montreal Neurological Institute; spatial resolution = 4 mm isotropic) to enable spatial comparison across subjects.

Z-statistic and signal change maps were calculated using the long-TE = 35 ms (TE2) data in three different ways: (i) for the entire BOLD dataset (TE2; 200 timepoints), (ii) only BOLD images (TE2) acquired after a control (no label) ASL acquisition (40 times-points), and (iii) only BOLD images (TE2) acquired after any ASL label (160 time-points; exclude only control preparation). Z-statistics were calculated to assess BOLD signal changes between the affected and unaffected, or less affected, hemisphere. Coregistered images were oriented such that radiological left was depicted as the primary affected hemisphere. For simplicity, the unaffected or less affected hemisphere will henceforth be referred to as the unaffected hemisphere.

Timecourses were calculated in gray matter within R ICA, L ICA, and VBA flow territories for each subject. Timecourses were extracted from BOLD-weighted images corresponding to each of the VE-ASL labeling scenarios, a total of 4, and the ASL control scenario. To reduce transition periods from biasing the calculations, baseline signals were taken from images acquired during the following time-points: 0–180 s, 450–540 s, and 810–900 s; active plateau signals were taken from images acquired during the following time-points: 270–360 s and 630–720 s. Baseline and active signals were not analyzed during periods of signal rise and fall as temporal differences influence signal intensities for the control and labeling conditions. Therefore, signal change comparisons were based on a total of 16 data

points for each labeling condition during room air administration (baseline) and a total of eight data points for each during carbogen administration. Consequently, even for relatively long stimulus durations (i.e., 3 min), the number of BOLD data points (i.e., no labeling) reduces to 8 when transition periods are excluded, thereby motivating the need to introduce strategies that may improve the temporal resolution of dual echo VE-ASL.

ASL Analysis

All CBF quantification was performed in Matlab. Surround subtractions were performed for the label and control images within each block and averaged. CBF maps were quantified in absolute units (mL/100 g/min) for both room air and carbogen inhalation by applying a two-compartment perfusion model (36) and using a constrained nonlinear optimization routine:

$$\Delta M=\frac{2M_0 f\alpha}{\lambda}\left\{\begin{array}{l}\frac{\exp(-\delta R_{1a})}{R_{1\mathrm{app}}}[\exp(\min(\delta-w,0)R_{1\mathrm{app}})-\exp((\delta-\tau-w)R_{1\mathrm{app}})]+\\ \frac{1}{R_{1a}}[\exp((\min(\delta_a-w,0)-\delta_a)R_{1a})-\exp((\min(\delta-w,0)-\delta)R_{1a})]\end{array}\right\} \quad [1]$$

where ΔM is the difference magnetization (control signal – label signal), M_0 is the equilibrium magnetization of tissue on a voxel-by-voxel basis to account for coil sensitivity, f is CBF (mL/100 g/min), $\alpha = 0.85$ is labeling efficiency for pCASL, $\lambda = 0.9$ mL/g is the blood-tissue water partition coefficient, $\delta = 1.5$ s is the tissue transit time (estimated here for patients with steno-occlusive disease), $R_{1a} = 0.59\ s^{-1}$ is the mean longitudinal relaxation rate of arterial blood water at 3.0T, $R_{1\mathrm{app}}$ = unperfused tissue R_1 ($0.77\ s^{-1}$)+f/λ, w = (1.600–2.240 s, or postlabeling delay [PLD] time, and accounts for the duration of the echo planar imaging readouts in the ascending slice acquisition, which is 0.060 s in the current dual echo implementation), $\tau = 1.5$ s the labeling pulse train duration, and $\delta_a = 0.5$ s is the arterial transit time. It should be noted that a range of R_{1b} values are reported in the literature (37–39), and the value chosen here is an approximation. During carbogen administration $R_{1b} = 0.73\ s^{-1}$, as the R_1 of arterial blood water decreases due to the physiological effects of hyperoxia (40,41), and $\delta = 1.425$s as the tissue transit time reduces by approximately 5% due to carbogen-associated vasodilation.

ASL images were transformed to standard space (4 mm isotropic resolution) by applying the same affine transformation matrix calculated from the BOLD images. Perfusion maps for the L ICA, R ICA, and VBA territories were calculated by applying a k-means clustering algorithm (32), with SNR threshold = 2.0, to the different labeling conditions.

Statistical Analysis

For each labeling scenario the BOLD signal intensities, percent signal changes, and Z-statistic values were compared for each perfusion territory. All statistical comparisons within each perfusion territory were calculated using paired t-tests relative to the respective values attained for the control scenario. Appropriate P-values to determine statistical significance were attained by Bonferroni corrections. Fifteen comparisons ($P \leq 0.003$) were made for percent signal changes and Z-statistics; while for Z-statistic comparisons between perfusion territories, 18 comparisons ($P \leq 0.002$) were made. Z-statistics were also assessed for potential correlations, using Spearman's rho, with CBF reactivity within each territory to assess the similarity between these measures during carbogen administration. Bartlett's test,

which reports homoscedasticity, was applied to the BOLD signal change maps to confirm how signal variance varied between regions with high and low Z-statistics.

RESULTS

Of the 23 patients scanned, 12 met inclusion criteria after grading of vasculopathy extent. Of these patients, 10 had a stenosis that was primarily flow-limiting to the left ICA territory and two had a stenosis that was primarily flow-limiting to the right ICA territory. When available, digital subtraction angiography (n = 6) images were used for vasculopathy measurements, otherwise magnetic resonance angiography (n = 5) or computed tomography angiography (n = 1) images were used. The average age of patients was 55 years (range = 35–80 years; s.d. = 14), with 6 females and 6 males. During scanning patients displayed an average $\Delta EtCO_2$ of 7.59 mmHg (s.d. = 1.95 mmHg). Patient demographics and characteristics are summarized in Table 1.

Figure 2 displays structural, BOLD CVR, and CBF data for an example patient (Patient 7, Table 1) who initially presented with 3 days of progressive confusion, apraxia, dyscalculia, and transient right-sided numbness. The patient had watershed infarcts of the left parietal and lateral occipital lobes. Presented data were acquired 4 months after initial inpatient visit; current data indicate left petrous/cavernous ICA (93%) and left M1 (74%) stenoses. In Figure 2a, the ischemic event is evidenced on both T1 and T2-FLAIR images in the left posterior parietal lobe. The dual echo VE-ASL sequence provides additional functional information regarding hemodynamic compromise. BOLD-derived CVR (Fig. 2b,c) demonstrated CVR asymmetry consistent with left ICA and left M1 stenoses, however, this is more obvious in the Z-statistic than the signal change map. Figure 2d shows the perfusion territory map along with baseline (room air) and hypercarbic hyperoxia (i.e., carbogen) CBF. The perfusion territory map is consistent with compensatory flow from the right ICA (green) to the left ICA territory (red), with only a small amount of blood being delivered from the heavily stenosed left ICA. CBF maps are approximately consistent with the BOLD reactivity maps, however, slight variations are present. An example BOLD timecourse (Fig. 2e) is shown, along with CVR summary statistics (Fig. 2f,g) for the different flow-labeling scenarios and when all labeling scenarios are analyzed together. The BOLD signal changes, calculated from long-TE VE-ASL data, for the different flow-labeling scenarios were not significantly different within either the affected or unaffected territories, indicating that spin labeling does not significantly affect relationships between impaired and unimpaired regions in the long-TE BOLD signal change maps. The Z-statistics were slightly higher for the VE conditions relative to the Control and Full labeling conditions.

For group analysis, we first considered the qualitative effect of the ASL labeling on BOLD CVR. BOLD Z-statistic maps normalized by $\Delta EtCO_2$ were calculated for all (n = 200) BOLD images, images acquired after any spin labeling prepulse (n = 160), and only after the control (nonlabeled) scenario (n = 40; Fig. 3). These maps indicated that all three groupings yielded similar BOLD-weighted contrast between affected and unaffected hemispheres (Fig. 3a), however, Z-statistics increase as the number of included images increases (Fig. 3b), as expected. This suggests that including all BOLD images in the analysis will provide statistically higher Z-statistics (and higher temporal resolution), yet the contrast to

lateralizing disease is not compromised owing to the very small effect of the spin labeling on the primarily T2*-weighted signal at long TE. Figure 4 shows corresponding group CBF maps for both room air (Fig. 4a) and carbogen (Fig. 4b) inhalation. To demonstrate the increase in CBF that is observed, the carbogen maps are not normalized by $\Delta EtCO_2$, but rather reflect CBF (ml/100 g/min). Figure 5a shows group BOLD and CBF reactivity maps. The CBF reactivity is defined as the CBF increase (ml/100 g/min) between room air breathing and carbogen breathing. Figure 5b shows scatter plots of BOLD and CBF reactivity data within all three territories of interest for all 12 subjects, along with the associated Spearman's rho. Correlations within the affected territory ($\rho = 0.76$, $P \leq 0.05$) were strongest, followed by the VBA territory ($\rho = 0.53$, $P \leq 0.05$). Correlations within the unaffected territory ($\rho = 0.37$, $P = 0.12$) were not significant. It should be noted that several patients displayed paradoxical findings, i.e., negative or negligible CBF and positive BOLD. When these patients were removed, the correlations were as follows: affected territory ($\rho = 0.66$, $P \leq 0.05$, two patients removed), VBA territory ($\rho = 0.65$, $P \leq 0.05$, one patient removed), unaffected territory ($\rho = 0.50$, $P = 0.07$, two patients removed). These data suggest BOLD Z-statistic and CBF correlations under carbogen administration varied for our experiment, but that with a sufficient range of values, as seen in the affected territory, these measures are similarly sensitive to reactivity; however, lateralization of reactivity is visually clearer in the BOLD CVR maps. Concerns regarding the relationship between BOLD and CBF CVR during carbogen administration are further addressed in the Discussion.

Figure 6 shows the mean timecourses across all volunteers, grouped separately for affected, unaffected, and VBA territories. The stimulus response is lower ($P \leq 0.003$ for all labeling conditions) in the affected region relative to the unaffected region for all flow-labeling conditions, and the posterior circulation timecourses are similar to the unaffected region timecourse, which is consistent with the posterior circulation being preserved in all patients (Table 1). These findings are presented quantitatively in Figure 7, Table 2, and Supporting Information Table 1.

Figure 7 and Supporting Information Table 1 demonstrate that BOLD signal changes did not differ between any of the label conditions relative to the control, nor did they differ when compared to the signal change calculated across the entire timecourse. Additionally, despite a trend the signal change did not differ significantly (Bonferroni corrected, $P>0.002$) between the affected, unaffected, or posterior territories for each of the labeling conditions, suggesting that BOLD signal changes in response to carbogen administration are not particularly sensitive to asymmetric cerebrovascular disease.

We also examined whether different trends were observed when Z-statistics instead of signal changes were considered (Fig. 7). Within each territory Z-statistics generated from the VE labeling conditions and the complete timecourse were significantly greater than those generated from the control scan (quantitative values provided in Supporting Information Table 1). Unlike signal changes, Z-statistics were sensitive ($P \leq 0.002$) to differences between the affected territory and the unaffected and VBA territory for all labeling conditions and the complete timecourse (Table 2).

Finally, Figure 8 indicates that the difference in sensitivity between BOLD signal change and BOLD Z-statistic maps in response to carbogen is that the latter is less sensitive to large intravascular signal variations in large vessels. As an example of this possibility, two ROIs (Fig. 8a) were chosen, one which incorporates a region of venous pooling near the outer layer of cortex (red arrow) and one located more medially that likely partial volumes with more microvasculature (blue arrow). These display different signal changes (blue: mean = 0.05, s.d. = 0.01; red: mean = 0.07, s.d. = 0.02) and Z-statistics (blue: mean- = 13.23, s.d. = 0.55; red: mean = 11.02, s.d. = 0.94) despite being very close in proximity and within a commonly impaired flow territory. Timecourses (Fig. 8b) were extracted from these ROIs and a Bartlett test was conducted to compare the variance of the baseline signal during room air (Fig. 8c) and carbogen inspiration (Fig. 8d). The Bartlett test indicated significantly greater variance under both room air ($X^2 = 22.0$; $P \leq 0.025$) and carbogen inspiration ($X^2 = 20.4$; $P \leq 0.025$), suggesting that Z-statistics may desensitize carbogen-induced CVR to nonspecific intravascular variance.

DISCUSSION

The current study examined the feasibility of implementing dual echo VE-ASL in a clinical setting with the aim of simultaneously delineating flow territories and assessing CBF- and BOLD-based reactivity in response to carbogen. The major findings of this study are (i) BOLD Z-statistics, but not signal changes, in response to carbogen are specific to lateralizing flow-limiting stenosis; (ii) CBF reactivity and BOLD reactivity (Z-statistics) in response to carbogen derived from the dual echo VE-ASL data correlate significantly, however, these correlations may depend on the reactivity range and may also extend to a paradoxical range in a small subgroup of patients (i.e., positive BOLD CVR with negligible or no CBF reactivity), and (iii) BOLD CVR (calculated as Z-statistics in response to all label and control conditions) from long-TE dual echo VE-ASL provides contrast consistent with lateralizing disease; furthermore, flow territories and CBF reactivity can be obtained from short-TE data, allowing for simultaneous measurement of flow territories, CBF reactivity, and BOLD reactivity in a clinical time frame (e.g., 15 min). In such a scan, the temporal resolution of the CBF measurement is approximately 8 s and that of the qualitative BOLD measurement can be as short as 4 s when all spin labeling conditions are included in analysis. The temporal resolution of the flow territory maps, which are derived from clustering applied to five different label/control scenarios, is approximately 4 min.

Advantages of Multiecho VE-ASL

The primary advantage of performing multiecho VE-ASL is that multiple sources of potential hemodynamic compromise can be derived in a single scan session. These include (i) baseline CBF, (ii) CBF response to vasodilatory stimulation, (iii) baseline flow territory, (iv) flow territory changes in response to vasodilatory stimulation, and (v) BOLD CVR. Additional metrics, such as quantitative R_2* mapping or functional connectivity analysis could in principle be performed as well, but were not specifically investigated in this study.

Including all labeling conditions in the BOLD analysis pipeline would have the additional benefit of obtaining a moderate BOLD temporal resolution (approximately 4 s), which is

important for assessing temporal CVR effects. For example, it may be beneficial to know whether a patient with lateralizing stenosis was experiencing regional delays in vascular reactivity, as this could provide potentially valuable information with regards to collateralization extent and even stroke risk. With the dual echo VE-ASL sequence implemented here, exclusion of the labeled BOLD images would result in a temporal resolution of 22.5 s, which may be insufficient to reveal the subtle differences necessary for such an analysis.

It was also of importance to understand the utility of the dual echo sequence for identifying regional impairment in cerebrovascular disease. Figure 2b–d depict CVR maps along with the calculated CBF maps and perfusion territories from a patient with left petrous/cavernous ICA and left M1 stenoses. A previous ischemic event in the left posterior parietal lobe is readily identifiable on both T1 and T2-FLAIR images; however, the extent of cerebrovascular impairment cannot be deduced. Areas of reduced CVR overlapping with the stroke region are evidenced on both Z-statistic and CBF images. Additionally, areas of reduced CVR extend anteriorly beyond the stroke site, as seen on T_2-weighted images, suggesting that other regions of intact brain parenchyma may be at risk for future stroke. Dual echo VE-ASL could also be used to facilitate longitudinal assessment as CBF provides a quantitative measure by which to monitor stenosis progression in regions supplied by the stenotic vessels, whereas Z-statistics are an alternative valuable tool for comparative assessment with respect to the contralateral hemisphere, as they appear less sensitive to hyperoxic effects in the draining vasculature, but may be influenced by variations in scanner stability. Furthermore, longitudinal monitoring of patients using standard contrast-based angiographic or perfusion imaging is difficult owing to inherent risks these invasive methods impose when performed serially.

Considerations of Dual Echo VE-ASL

Several complications of dual echo VE-ASL should also be considered when choosing the most appropriate method for a given application. First, the spatial and temporal resolutions of long-TE BOLD images were restricted by the parameters necessary for pCASL. Specifically, the application of the labeling pulses and the inversion time contribute substantially to lower BOLD temporal resolution. This resulted in a reduction of temporal resolution by approximately 2.5 s at 3T, even when all labeling conditions were included in BOLD analysis. With the block design implemented in the current experiment and the robust, global effects that were expected, this degree of reduction in temporal resolution was not problematic.

Second, to avoid further increases in TR and to maintain reasonable ASL SNR (required especially for flow territory mapping), a slice thickness of 7 mm was used. As BOLD-weighted imaging is based on susceptibility differences, susceptibility artifacts in the frontal sinuses are more prominent due to the partial voluming of spins with differential phase within larger voxels. Artifacts are further exacerbated during hypercarbic hyperoxia inhalation as hyperoxia creates greater susceptibility differences. Therefore, we observed slightly greater dropout and distortion in lower regions of the frontal lobes than may be observed in independently acquired BOLD scans with high spatial resolution and short-TE

pCASL scans. As such, one may consider using a shorter TE2. This is not ideal, however, as the TE for BOLD-weighted imaging should be approximately set to the T_2* of the tissue (42), otherwise data will be more significantly weighted by intravascular signal relative to tissue signal.

Third, as the cortical ASL perfusion signal is generally less than 1% higher than the static background signal, ASL can benefit from the application of background suppression to null the longitudinal magnetization of static tissue signal (43). Application of background suppression, however, significantly reduces BOLD SNR in a slice-dependent fashion. Accordingly, we chose to exclude the application of background suppression pulses to avoid possible detrimental effects to our analyses. Nevertheless, the resulting short-TE (flow-weighted) images provided sufficient SNR to examine vascular responses to the gas challenge. Recent evidence suggests that reduction of BOLD SNR as a result of background suppression application during dual echo ASL does not significantly decrease the sensitivity of the BOLD contrast as measured by Z-statistics (44). The resulting Z-statistics, however, are slice dependent as the effect of the background suppression reduces with increasing slice number, but this could potentially be resolved through postprocessing strategies. Therefore, application of background suppression inversion pulses during multiecho VE-ASL may be considered in order to improve ASL SNR and interpretability while maintaining the appropriate BOLD contrast, however, this requires verification.

Fourth, one of the most desirable advantages of planning-free dual echo VE-ASL is that it allows for flow territory mapping without time-consuming preparations. However, CBF should likely not be calculated from the vessel-specific scenarios. Specifically, the accuracy of CBF quantification is reduced where inflowing blood-water from the labeled vessel mixes with inflowing blood-water from unlabeled vessels when using k-means clustering methods to delineate territories, as was performed here. Recent work indicates that planning-free VE-ASL flow territory quantification may be significantly improved when supplementing k-means clustering with a linear fit to improve the estimated labeling efficiency at each voxel, or by generating flow territory maps within a Bayesian framework, which may be more sensitive to mixing (45).

Fifth, our data indicate a possible vessel-encoding dependent effect on BOLD calculated Z-statistics, but not signal change. Specifically, Figure 7 shows that Z-statistics are slightly increased for BOLD images acquired after vessel-selective labeling relative to the nonspecific (full) label or the control scan. This observation is also apparent in the example patient shown in Figure 2. While the origins of this finding are unclear, we believe this effect may be due to reduced variance as a result of the vessel-specific preparations. In other words, spin labeling reduces the intravascular longitudinal magnetization, which results in reduced intravascular signal and variance, which could increase the Z-statistic. Conversely, with the full labeling condition, an overall reduction in SNR may partially offset this effect. A point of future work, which would have ramifications beyond just spin labeling and CBF quantification, would be to evaluate whether spin labeling preparations are capable of increasing BOLD Z-statistics through a reduction in intravascular signal variance.

Lastly, the use of a hypercarbic hyperoxic (e.g., carbogen) stimulus, rather than a standard hypercarbic mixture (21% O_2, 5% CO_2, and 74% N_2), will lead to significant increases in FiO_2, resulting in increased blood [HbO_2], which will occur in veins and may extend to arteries in patients with low arterial blood oxygen saturation at baseline. Importantly, these limitations are related specifically to the carbogen challenge rather than the general VE-ASL method. However, the study population here comprised patients with ischemic steno-occlusive disease, many of whom likely have elevated oxygen extraction fractions and low sPO_2. It is unclear whether exposing these patients to standard hypercarbic mixtures (i.e., hypercarbia with a balance of normoxic air) will exacerbate symptoms or even induce ischemia in patients operating near reserve capacity. Therefore, due to safety concerns, our hospital required a hypercarbic gas mixture that would clearly increase oxygen delivery to tissue. Future work is warranted to determine the safety and utility of using hypercarbic gas mixtures in subacute and early chronic patients.

In light of this confound, we observed that evaluation of Z-statistics provide contrast visually consistent with lateralizing disease, where the signal changes were heavily biased by what appears to be draining veins (Figure 8c,d). We have also demonstrated abilities to identify lateralizing disease using this approach and these values are largely consistent with CBF reactivity (Fig. 5). It should be noted that hypercarbic hyperoxia will elicit changes in CVR, through the hypercarbic fraction of the stimulus, as well as increases in blood oxygenation, owing to the hyperoxic component of the stimulus. The fraction of O_2 that is dissolved in plasma will not contribute directly to BOLD signal, but, increases in [HbO_2] relative to [dHb] due to hyperoxia will contribute to BOLD signal in a manner that does not depend on CVR. Hyperoxia, however, has been shown to have a small-to-negligible reduction in CBF and CBV when administered for short durations. These two assumptions together suggest that carbogen-induced BOLD CVR should be systematically increased relative to hypercarbic normoxic-induced BOLD CVR, but it is not necessarily expected that the two should be unrelated.

Our results (Fig. 5b) indicate BOLD (Z-statistic) and CBF reactivity correlate during carbogen stimulation. This finding is strongest in the affected hemisphere where there is a larger dynamic range of measurements. This finding differs from work by others where BOLD and ASL CVR were compared for carbogen administration (46). There are several possible reasons for this discrepancy. First, for pCASL, the recommended PLD ranges from 1500 to 2000 ms to allow sufficient time for the inverted blood water to exchange with the tissue compartment. We used a PLD time of 1600 ms, within the recommended range. In (46), however, a PLD of 800 ms was used. At such a short PLD, it is expected that a substantial fraction of labeled blood water remains within the feeding vasculature, which drastically increases the sensitivity of the ASL signal to intravascular effects where the artifact from carbogen is expected to be highest. Second, as demonstrated by BOLD signal changes in Figure 6b,c, it takes approximately 30–45 s for the carbogen-induced BOLD effect to plateau in healthy tissue, and even longer in ischemic tissue (Fig. 6a), while it also takes at least 30–45 s for the baseline signal to stabilize after the carbogen stimulus is suspended. As such, we chose 3 min (180 s) durations to allow BOLD and ASL readout of the stable baseline and carbogen signals, to minimize the effect of rising and falling signal from our analyses which would have introduced greater variability into our results. These

transitionary periods were incorporated in the analysis and modeled in (46) given that baseline and activation blocks were only of 1 min duration. Third, in (46) only healthy CVR was analyzed, which may provide a very narrow range for correlation analyses to be performed. Here, we demonstrated similar effects in the unimpaired ICA territory, but demonstrated significant correlations within the affected ICA territory where there is a larger dynamic range of measurements.

Paradoxical BOLD and CBF findings in our study could also be explained by long bolus arrival times in some patients, which result in large intravascular blood water signal at typical postlabeling delay times. During stimulation (i.e., carbogen), the bolus arrival time reduces slightly and more blood water may exchange with tissue water; this could lower the perfusion signal relative to the baseline signal which contained large intravascular blood water signal. This effect, however, could have been significantly reduced by the use of flow crushing gradients which would have reduced ASL sensitivity to the intravascular blood water signal. We deliberately did not use vascular crusher gradients in our study due to concerns that crusher gradients would (i) lengthen the TE and lower SNR, (ii) provide incomplete crushing when performed in only one direction, or otherwise considerably increase TE if applied sequentially in all directions, and (iii) provide variable sensitivity to delayed or low-velocity flow. Therefore, this effect is not necessarily specific to hypercarbic hyperoxia as opposed to hypercarbic normoxia administration. Relatedly, we also accounted for a blood water R_1 change with hyperoxia in our CBF quantification. While the value used here was independently measured by us (40) and similar to what is used by other groups (41), this value will depend on FiO_2 and pO_2, which may vary from patient to patient, and this could cause a paradoxical CBF reactivity measurement if the estimate is sufficiently far from the true value. This confound is most prominent for carbogen, and it may be evident to a smaller extent for hypercarbic normoxic stimuli if ventilation changes substantially. Overall, where quantitative BOLD physiology is of interest, and in patients where a need to increase FiO_2 is not required, hypercarbic normoxic challenges are more straightforward to interpret.

CONCLUSIONS

Planning-free dual echo VE-ASL performed during carbogen administration can provide simultaneous CBF and qualitative BOLD contrast consistent with lateralizing disease severity in patients with asymmetric steno-occlusive disease when appropriate postprocessing strategies are implemented.

Supplementary Material

Refer to Web version on PubMed Central for supplementary material.

References

1. Bokkers RP, van Osch MJ, Klijn CJ, Kappelle LJ, Hendrikse J. Cerebrovascular reactivity within perfusion territories in patients with an internal carotid artery occlusion. J Neurol Neurosurg Psychiatry. 2011; 82:1011–1016. [PubMed: 21386110]

2. Detre JA, Alsop DC, Vives LR, Maccotta L, Teener JW, Raps EC. Noninvasive MRI evaluation of cerebral blood flow in cerebrovascular disease. Neurology. 1998; 50:633–641. [PubMed: 9521248]
3. Donahue MJ, Ayad M, Moore R, van Osch M, Singer R, Clemmons P, Strother M. Relationships between hypercarbic reactivity, cerebral blood flow, and arterial circulation times in patients with moyamoya disease. J Magn Reson Imaging. 2013; 38:1129–1139. [PubMed: 23440909]
4. Hendrikse J, Petersen ET, Cheze A, Chng SM, Venketasubramanian N, Golay X. Relation between cerebral perfusion territories and location of cerebral infarcts. Stroke. 2009; 40:1617–1622. [PubMed: 19299630]
5. Van Laar PJ, Hendrikse J, Mali WP, Moll FL, van der Worp HB, van Osch MJ, van der Grond J. Altered flow territories after carotid stenting and carotid endarterectomy. J Vasc Surg. 2007; 45:1155–1161. [PubMed: 17543680]
6. Zaharchuk G, Do HM, Marks MP, Rosenberg J, Moseley ME, Steinberg GK. Arterial spin-labeling MRI can identify the presence and intensity of collateral perfusion in patients with moyamoya disease. Stroke. 2011; 42:2485–2491. [PubMed: 21799169]
7. Wintermark M, Reichhart M, Thiran JP, Maeder P, Chalaron M, Schnyder P, Bogousslavsky J, Meuli R. Prognostic accuracy of cerebral blood flow measurement by perfusion computed tomography, at the time of emergency room admission, in acute stroke patients. Ann Neurol. 2002; 51:417–432. [PubMed: 11921048]
8. Detre JA, Leigh JS, Williams DS, Koretsky AP. Perfusion imaging. Magn Reson Med. 1992; 23:37–45. [PubMed: 1734182]
9. Williams DS, Detre JA, Leigh JS, Koretsky AP. Magnetic resonance imaging of perfusion using spin inversion of arterial water. Proc Natl Acad Sci USA. 1992; 89:212–216. [PubMed: 1729691]
10. Silva AC, Kim SG. Pseudo-continuous arterial spin labeling technique for measuring CBF dynamics with high temporal resolution. Magn Reson Med. 1999; 42:425–429. [PubMed: 10467285]
11. Wong EC, Buxton RB, Frank LR. Implementation of quantitative perfusion imaging techniques for functional brain mapping using pulsed arterial spin labeling. NMR Biomed. 1997; 10:237–249. [PubMed: 9430354]
12. Hendrikse J, van der Grond J, Lu H, van Zijl PC, Golay X. Flow territory mapping of the cerebral arteries with regional perfusion MRI. Stroke. 2004; 35:882–887. [PubMed: 14988567]
13. Wong EC. Vessel-encoded arterial spin-labeling using pseudocontinuous tagging. Magn Reson Med. 2007; 58:1086–1091. [PubMed: 17969084]
14. Okell TW, Chappell MA, Kelly ME, Jezzard P. Cerebral blood flow quantification using vessel-encoded arterial spin labeling. J Cereb Blood Flow Metab. 2013; 33:1716–1724. [PubMed: 23921895]
15. Chen JJ, Pike GB. Global cerebral oxidative metabolism during hypercapnia and hypocapnia in humans: implications for BOLD fMRI. J Cereb Blood Flow Metab. 2010; 30:1094–1099. [PubMed: 20372169]
16. Davis TL, Kwong KK, Weisskoff RM, Rosen BR. Calibrated functional MRI: mapping the dynamics of oxidative metabolism. Proc Natl Acad Sci USA. 1998; 95:1834–1839. [PubMed: 9465103]
17. Hoge RD, Atkinson J, Gill B, Crelier GR, Marrett S, Pike GB. Investigation of BOLD signal dependence on cerebral blood flow and oxygen consumption: the deoxyhemoglobin dilution model. Magn Reson Med. 1999; 42:849–863. [PubMed: 10542343]
18. Wise RG, Harris AD, Stone AJ, Murphy K. Measurement of OEF and absolute CMRO2: MRI-based methods using interleaved and combined hypercapnia and hyperoxia. Neuroimage. 2013; 83:135–147. [PubMed: 23769703]
19. Zappe AC, Uludag K, Oeltermann A, Ugurbil K, Logothetis NK. The influence of moderate hypercapnia on neural activity in the anesthetized nonhuman primate. Cereb Cortex. 2008; 18:2666–2673. [PubMed: 18326521]
20. Ito H, Kanno I, Ibaraki M, Hatazawa J, Miura S. Changes in human cerebral blood flow and cerebral blood volume during hypercapnia and hypocapnia measured by positron emission tomography. J Cereb Blood Flow Metab. 2003; 23:665–670. [PubMed: 12796714]

21. Ito H, Ibaraki M, Kanno I, Fukuda H, Miura S. Changes in the arterial fraction of human cerebral blood volume during hypercapnia and hypocapnia measured by positron emission tomography. J Cereb Blood Flow Metab. 2005; 25:852–857. [PubMed: 15716851]
22. Wise RG, Pattinson KT, Bulte DP, Rogers R, Tracey I, Matthews PM, Jezzard P. Measurement of relative cerebral blood volume using BOLD contrast and mild hypoxic hypoxia. Magn Reson Imaging. 2010; 28:1129–1134. [PubMed: 20685053]
23. Hajjar I, Zhao P, Alsop D, Abduljalil A, Selim M, Novak P, Novak V. Association of blood pressure elevation and nocturnal dipping with brain atrophy, perfusion and functional measures in stroke and nonstroke individuals. Am J Hypertens. 2010; 23:17–23. [PubMed: 19798036]
24. Haller S, Bonati LH, Rick J, Klarhofer M, Speck O, Lyrer PA, Bilecen D, Engelter ST, Wetzel SG. Reduced cerebrovascular reserve at CO2 BOLD MR imaging is associated with increased risk of periinterventional ischemic lesions during carotid endarterectomy or stent placement: preliminary results. Radiology. 2008; 249:251–258. [PubMed: 18796680]
25. Heyn C, Poublanc J, Crawley A, Mandell D, Han JS, Tymianski M, terBrugge K, Fisher JA, Mikulis DJ. Quantification of cerebrovascular reactivity by blood oxygen level-dependent MR imaging and correlation with conventional angiography in patients with Moyamoya disease. AJNR Am J Neuroradiol. 2010; 31:862–867. [PubMed: 20075092]
26. Mandell DM, Han JS, Poublanc J, Crawley AP, Fierstra J, Tymianski M, Fisher JA, Mikulis DJ. Quantitative measurement of cerebrovascular reactivity by blood oxygen level-dependent MR imaging in patients with intracranial stenosis: preoperative cerebrovascular reactivity predicts the effect of extracranial-intracranial bypass surgery. AJNR Am J Neuroradiol. 2011; 32:721–727. [PubMed: 21436343]
27. van Laar PJ, van Raamt AF, van der Grond J, Mali WP, van der Graaf Y, Hendrikse J, Group SS. Increasing levels of TNFalpha are associated with increased brain perfusion. Atherosclerosis. 2008; 196:449–454. [PubMed: 17222850]
28. Lu H, Donahue MJ, van Zijl PC. Detrimental effects of BOLD signal in arterial spin labeling fMRI at high field strength. Magn Reson Med. 2006; 56:546–552. [PubMed: 16894581]
29. Perthen JE, Bydder M, Restom K, Liu TT. SNR and functional sensitivity of BOLD and perfusion-based fMRI using arterial spin labeling with spiral SENSE at 3 T. Magn Reson Imaging. 2008; 26:513–522. [PubMed: 18158226]
30. Woolrich MW, Chiarelli P, Gallichan D, Perthen J, Liu TT. Bayesian inference of hemodynamic changes in functional arterial spin labeling data. Magn Reson Med. 2006; 56:891–906. [PubMed: 16964610]
31. Donahue MJ, Hussey E, Rane S, Wilson T, van Osch M, Hartkamp N, Hendrikse J, Ally BA. Vessel-encoded arterial spin labeling (VE-ASL) reveals elevated flow territory asymmetry in older adults with substandard verbal memory performance. J Magn Reson Imaging. 2013; 39:377–386. [PubMed: 23633160]
32. Gevers S, Bokkers RP, Hendrikse J, Majoie CB, Kies DA, Teeuwisse WM, Nederveen AJ, van Osch MJ. Robustness and reproducibility of flow territories defined by planning-free vessel-encoded pseudocontinuous arterial spin-labeling. AJNR Am J Neuroradiol. 2012; 33:E21–25. [PubMed: 21393410]
33. Smith SM, Jenkinson M, Woolrich MW, et al. Advances in functional and structural MR image analysis and implementation as FSL. Neuroimage. 2004; 23(Suppl 1):S208–S219. [PubMed: 15501092]
34. Woolrich MW, Jbabdi S, Patenaude B, Chappell M, Makni S, Behrens T, Beckmann C, Jenkinson M, Smith SM. Bayesian analysis of neuroimaging data in FSL. Neuroimage. 2009; 45(1 Suppl):S173–S186. [PubMed: 19059349]
35. Donahue MJ, Hoogduin H, Smith SM, Siero JC, Chappell M, Petridou N, Jezzard P, Luijten PR, Hendrikse J. Spontaneous blood oxygenation level-dependent fMRI signal is modulated by behavioral state and correlates with evoked response in sensorimotor cortex: a 7. 0-T fMRI study. Hum Brain Mapp. 2012; 33:511–522. [PubMed: 21455940]
36. Wang J, Alsop DC, Li L, Listerud J, Gonzalez-At JB, Schnall MD, Detre JA. Comparison of quantitative perfusion imaging using arterial spin labeling at 1.5 and 4. 0 Tesla. Magn Reson Med. 2002; 48:242–254. [PubMed: 12210932]

37. Lu H, Clingman C, Golay X, van Zijl PC. Determining the longitudinal relaxation time (T1) of blood at 3.0 Tesla. Magn Reson Med. 2004; 52:679–682. [PubMed: 15334591]

38. Zhang X, Petersen ET, Ghariq E, De Vis JB, Webb AG, Teeuwisse WM, Hendrikse J, van Osch MJ. In vivo blood T(1) measurements at 1. 5 T, 3 T, and 7 T. Magn Reson Med. 2013; 70:1082–1086. [PubMed: 23172845]

39. Varela M, Hajnal JV, Petersen ET, Golay X, Merchant N, Larkman DJ. A method for rapid in vivo measurement of blood T1. NMR Biomed. 2011; 24:80–88. [PubMed: 20669148]

40. Dethrage, LM.; Faraco, CC.; Strother, MK.; Donahue, MJ. In vivo quantification of blood water R_1 change during hypercarbic hyperoxia. Proceedings of the 22nd Annual Meeting of ISMRM; Milan, Italy. 2014. p. 4558

41. Bulte DP, Chiarelli PA, Wise RG, Jezzard P. Cerebral perfusion response to hyperoxia. J Cereb Blood Flow Metab. 2007; 27:69–75. [PubMed: 16670698]

42. Donahue MJ, Hoogduin H, van Zijl PC, Jezzard P, Luijten PR, Hendrikse J. Blood oxygenation level-dependent (BOLD) total and extravascular signal changes and DeltaR2* in human visual cortex at 1.5, 3.0 and 7. 0 T. NMR Biomed. 2011; 24:25–34. [PubMed: 21259367]

43. Ye FQ, Frank JA, Weinberger DR, McLaughlin AC. Noise reduction in 3D perfusion imaging by attenuating the static signal in arterial spin tagging (ASSIST). Magn Reson Med. 2000; 44:92–100. [PubMed: 10893526]

44. Ghariq, E.; Chappell, MA.; Schmid, S.; Teeuwisse, WM.; van Buchem, MA.; Webb, AG.; van Osch, MJ. Effects of background suppression on the sensitivity of dual-echo arterial spinl labeling MRI for BOLD and CBF signal changes. Proceedings of the 20th Annual Meeting of ISMRM; Melbourne, Australia. 2012. p. 3497

45. Hartkamp NS, Helle M, Chappell MA, Okell TW, Hendrikse J, Bokkers RP, van Osch MJ. Validation of planning-free vessel-encoded pseudo-continuous arterial spin labeling MR imaging as territorial-ASL strategy by comparison to super-selective p-CASL MRI. Magn Reson Med. 2014; 71:2059–2070. [PubMed: 23878062]

46. Hare HV, Germuska M, Kelly ME, Bulte DP. Comparison of CO2 in air versus carbogen for the measurement of CVR with magnetic resonance imaging. J Cereb Blood Flow Metab. 2013; 33:1799–1805. [PubMed: 23921896]

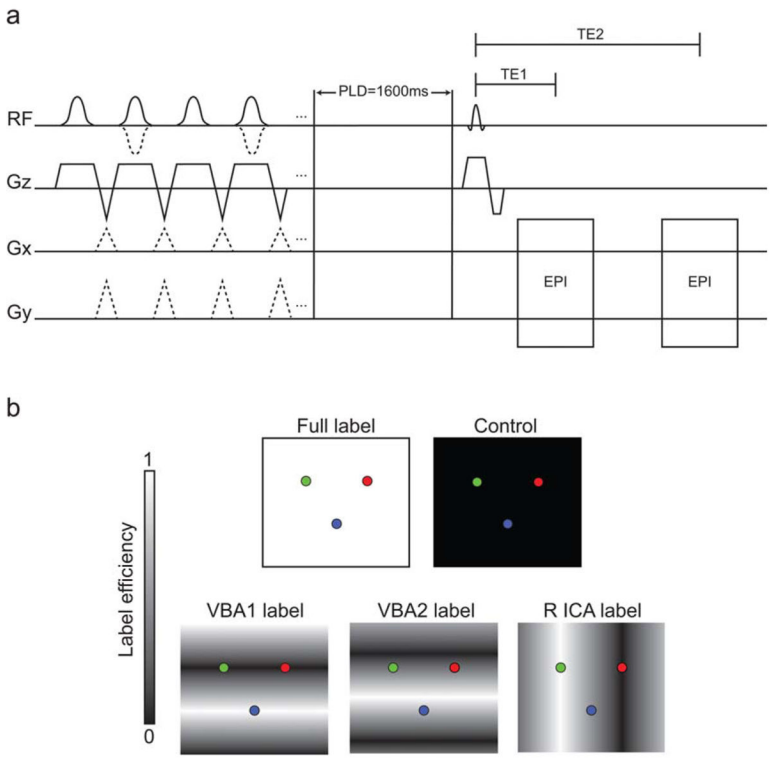

FIG. 1.

Dual echo VE-ASL and BOLD pulse sequence. **a:** The first half of the diagram, before the post-labeling delay (PLD), depicts the labeling pulse train for each of the pCASL labeling scenarios and the control. A series of Hanning-windowed pulses (pulse duration = 0.5 ms) were used for blood water labeling. The control scan is achieved through use of consecutive radiofrequency pulses with alternating polarity, the full label only requires the slice-select gradient, while each VE label is achieved by application of interpulse transverse (Gx and Gy) gradients. In this protocol, four separate labeling conditions were performed along with one control condition. Each pulse train is followed by a 1600 ms PLD. Acquisition occurs with two single-shot gradient echo planar imaging readouts, with TE 1 corresponding to the readout with low BOLD sensitivity (TE1 = 10.5 ms) and TE 2 corresponding to the BOLD-weighted readout (TE2 = 35 ms). **b:** Ideal labeling efficiency of the different ASL labeling conditions. From left to right, the top row depicts the full label (white background) and control (black background) pulses, whereas the bottom row depicts the VBA and ICA conditions: VBA1, VBA2, and R ICA.

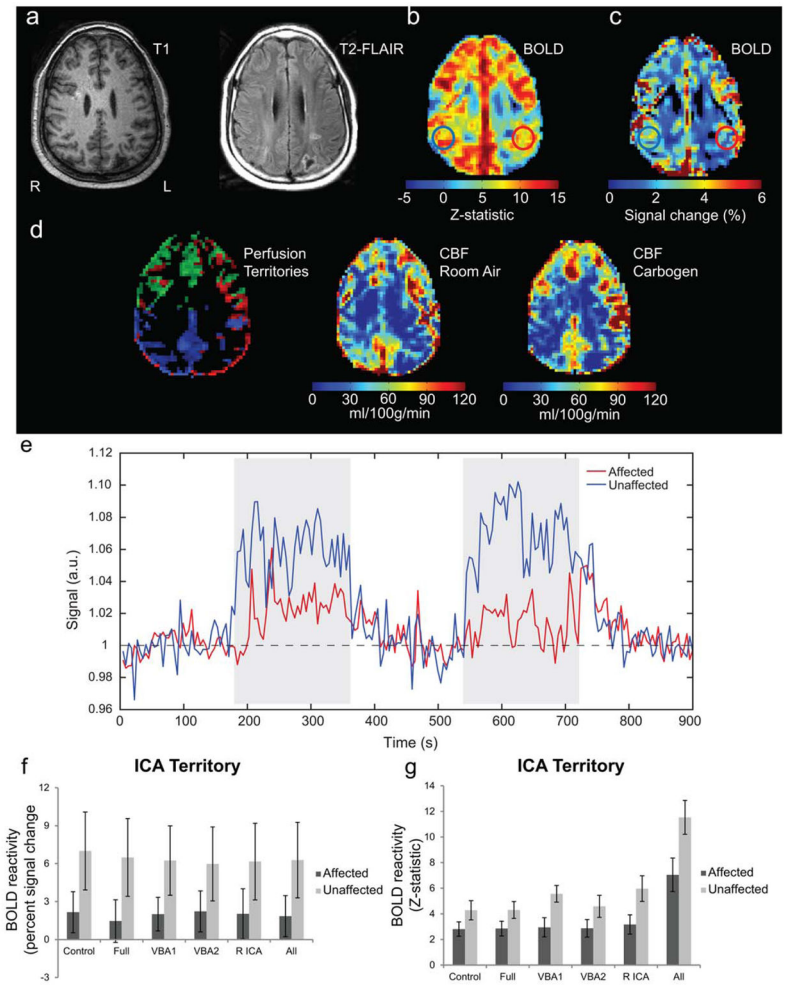

FIG. 2.

Single patient example demonstrating the information available from the dual echo VE-ASL sequence even in cases of excessive motion. A 46-year-old male (Patient 7, Table 1) with left petrous/cavernous ICA and left M1 stenoses. **a:** T1 and T2-FLAIR images depict a left posterior parietal region which suffered a previous ischemic event related to the L petrous/cavernous ICA/M1 stenoses. **b:** BOLD Z-statistic image which demonstrates the ability of the long-TE images to identify lateralizing contrast consistent with the stenosis. **c:** BOLD signal change map for the same slice; hemispheric asymmetry, however, is not as evident as in the Z-statistics. **d:** Perfusion territory along with baseline and carbogen CBF maps demonstrate the impact of ischemia on surrounding tissue. The perfusion territory map, however, indicates the R ICA is partly supplying the left hemisphere. **e:** Corresponding timecourse plots for the affected and unaffected regions. Notice a delay in the rise of the BOLD signal and overall lower CVR in the affected ICA territory. Together, these data demonstrate the additional information that can be provided by BOLD and ASL imaging in patients. **f:** Corresponding percent signal changes grouped by control and ASL labeling (Full, VBA1, VBA2, R ICA, and all labeling conditions combined) for the ICA territory regions identified in the signal change image. All signal changes were significantly greater

($P \leq 0.01$, Bonferroni corrected) in the unaffected territory compared to the affected territory. **g:** Corresponding BOLD Z-statistics grouped by control and ASL labeling pulses (Full, VBA1, VBA2, R ICA, and all labeling conditions combined) for the ICA territory regions identified in the BOLD image. These images are also sensitive ($P \leq 0.01$, Bonferroni corrected) to hemispheric asymmetry, but display a sensitivity ($P \leq .006$, Bonferroni corrected) to the labeling pulses (VBA1 and R ICA) not seen in the signal change maps (see Discussion).

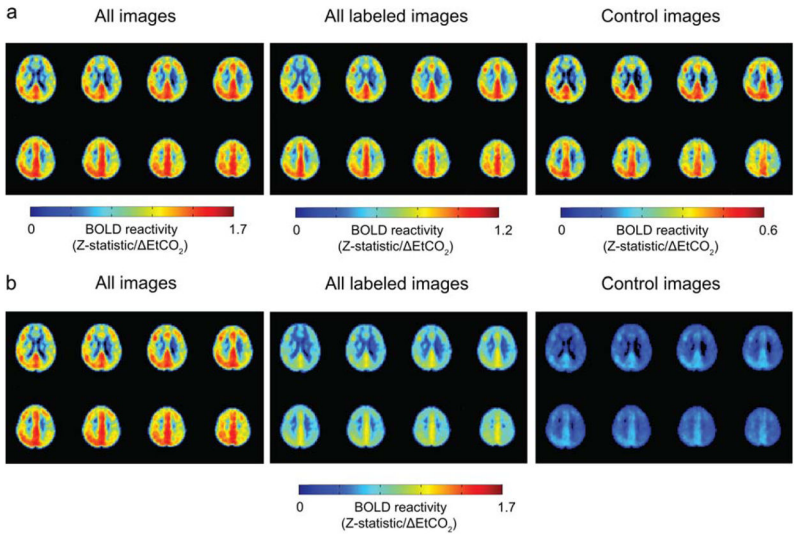

FIG. 3.

Group BOLD Z-statistics, normalized by the end-tidal CO_2 change ($\Delta EtCO_2$), with affected hemisphere on radiological left. **a:** Normalized Z-statistic maps calculated from all labeling and control conditions, images acquired after only labeling conditions (Full, VBA1, VBA2, and R ICA), and images acquired after the control condition only. **b:** The same normalized Z-statistics as in (a)**,** but scaled at the same intensity to demonstrate the difference in statistical power gained when calculating statistics using all BOLD images.

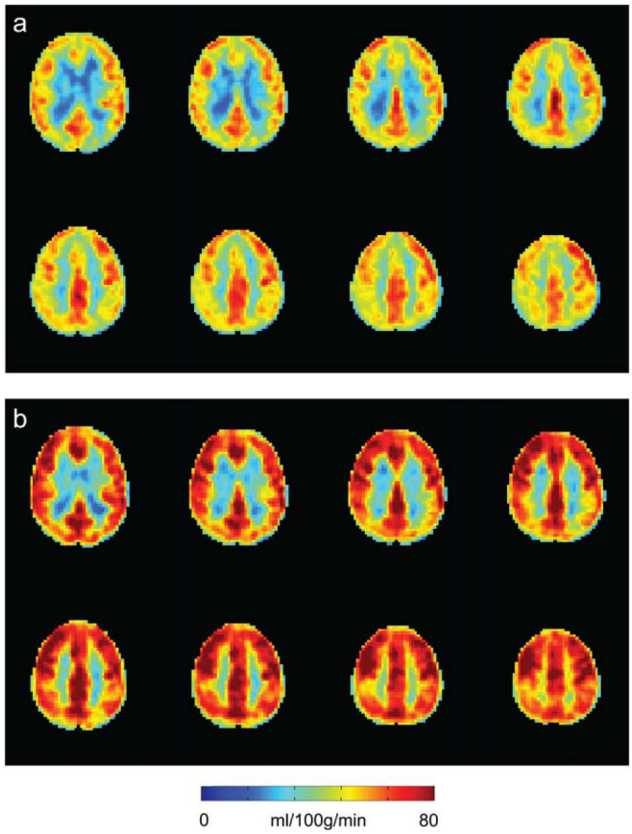

FIG. 4.

Group CBF maps with affected hemisphere on radiological left. **a:** Mean baseline CBF. **b:** Mean CBF during carbogen.

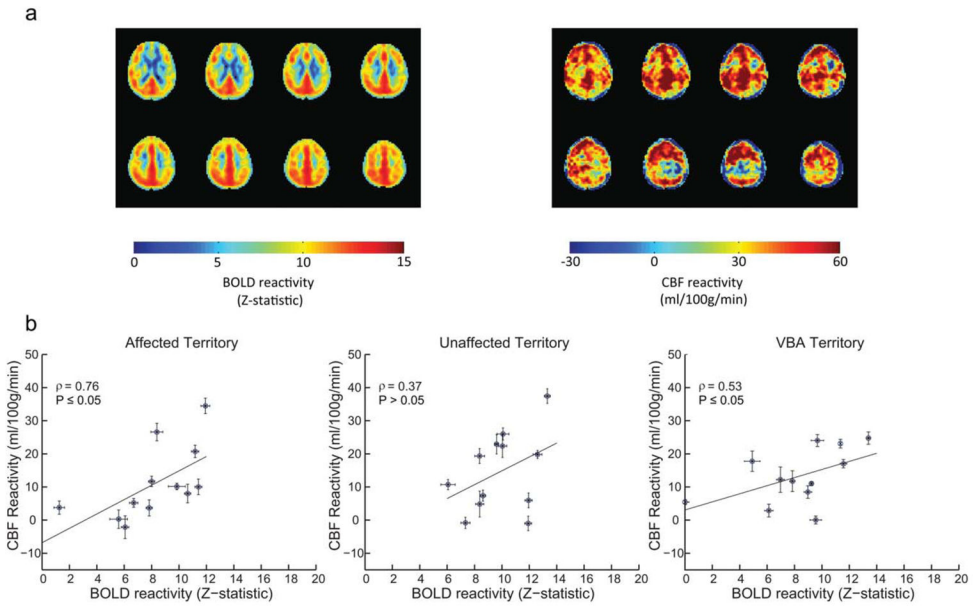

FIG. 5.

BOLD and CBF reactivity maps along with associated correlations within each territory. **a:** Group-wise BOLD and CBF reactivity, respectively. **b:** Scatter plot data, for all 12 subjects, between BOLD and CBF reactivity within each territory of interest, along with the associated Spearman's rho. Correlations were strongest within the affected ICA territory ($\rho = 0.76$, $P \leq 0.05$), followed by the VBA territory ($\rho = 0.53$, $P \leq 0.05$). Correlations for the unaffected ICA territory ($\rho = 0.37$, $P > 0.05$) were significant. Error bars represent the standard error. It should be noted that two patients presented with negative or nearly null CBF reactivity but positive BOLD reactivity in the affected hemisphere, which is addressed in the Discussion. Similarly two patients demonstrated similar patterns for the unaffected ICA territory, and one patient demonstrated this in VBA territory. When patients with such negative/null CBF reactivity were excluded from the analysis correlation values reduced slightly to $\rho = 0.66$ ($P \leq 0.05$) for the affected territory, and increased to $\rho = 0.65$ ($P \leq 0.05$) and $\rho = 0.50$ ($P = 0.07$) for the VBA and unaffected ICA territories, respectively.

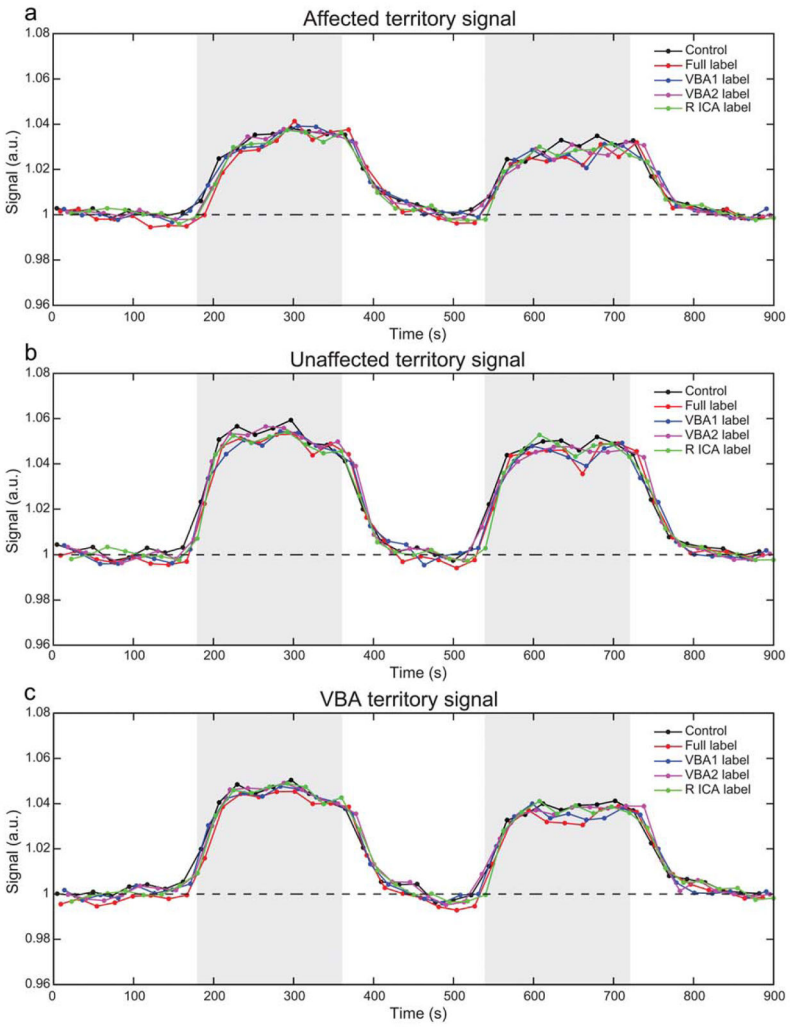

FIG. 6.

Timecourse plots per perfusion territory and labeling scheme. **a–c:** Plots depict the average BOLD timecourse for each perfusion territory decomposed based on the ASL scheme for the affected territory, unaffected territory, and VBA territory, respectively. Blocks of carbogen inspiration are shaded in gray. Full label refers to labeling of all inflowing vessels.

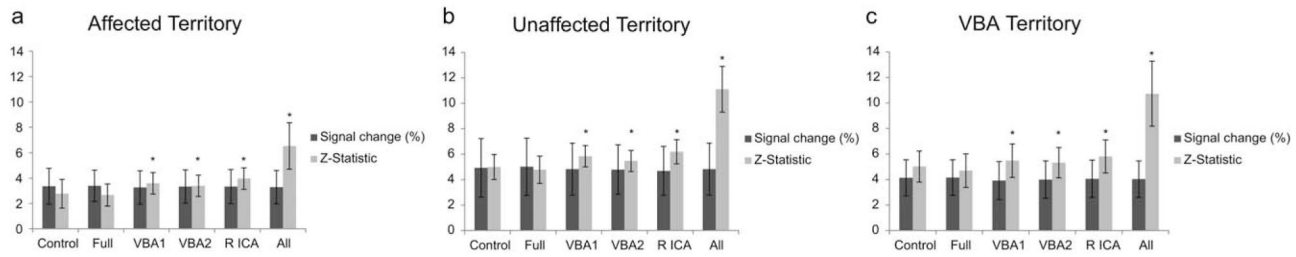

FIG. 7.

BOLD percent signal change and Z-statistics per perfusion territory and labeling condition. **(a), (b),** and **(c)** depict BOLD groupwise signal changes and Z-statistics calculated from images acquired after the nonlabeling condition (Control), each ASL labeling condition (Full, VBA1, VBA2, and R ICA pulses), and all images (all label and control conditions) from the series for the affected territory, the unaffected territory, and the VBA territory, respectively. T-tests within each region demonstrate that the ASL labeling preparation does not significantly affect the BOLD-weighted signal change with respect to the control scan in any of the perfusion territories. T-tests with respect to attained Z-statistic values, however, indicate that Z-statistics demonstrate some sensitivity to the ASL labeling pulse. * indicates value is significantly different ($P \leq 0.002$, Bonferroni corrected) relative to Control value.

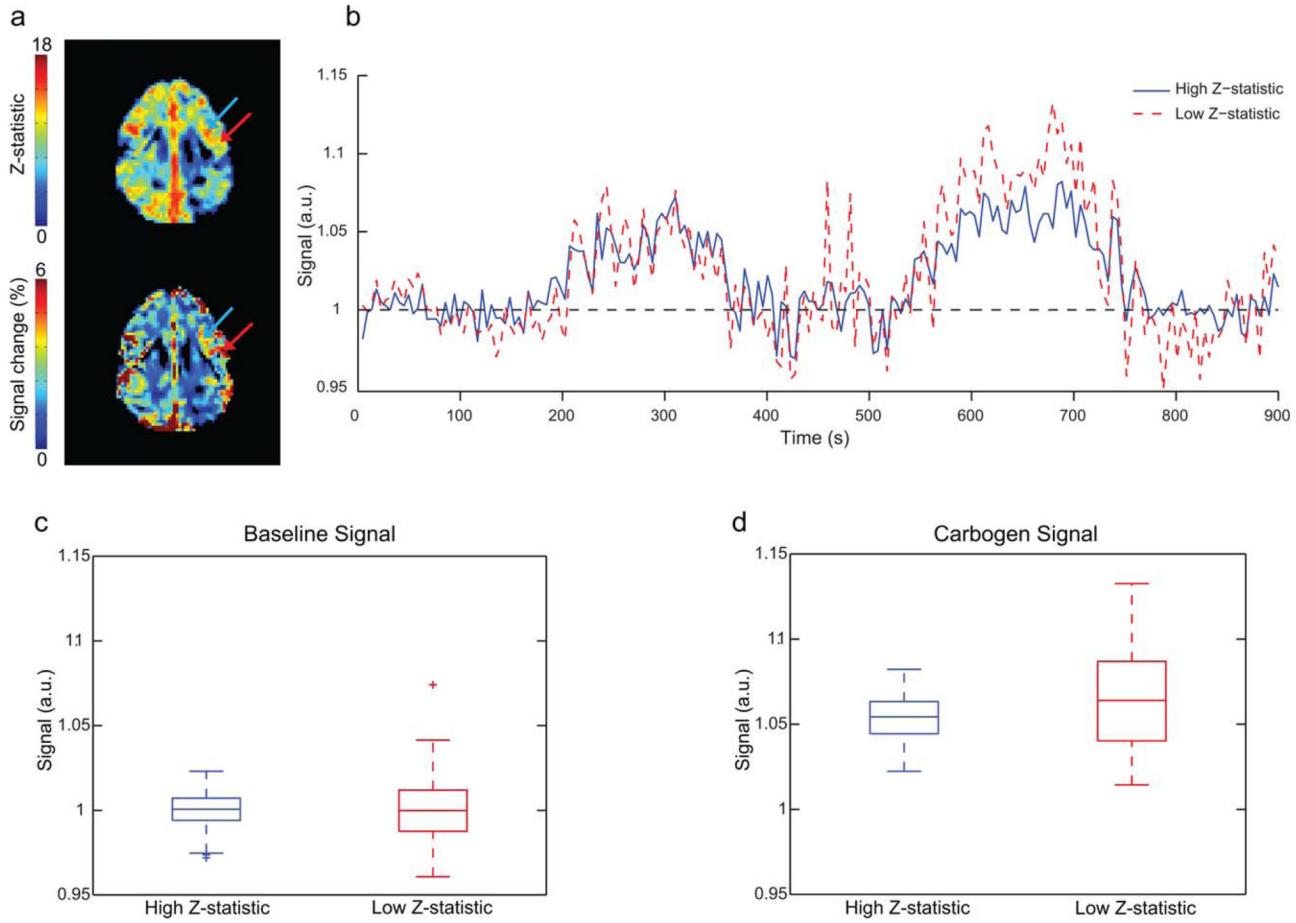

FIG. 8.

Relationship between signal variation and BOLD signal change and Z-statistic. **a:** Z-statistic (top) and signal change (bottom) maps for the case example presented in Figure 2. The blue arrow corresponds to a region of higher Z-statistics but lower signal change, whereas the red arrow corresponds to a region of lower Z-statistics but higher signal change. The red arrow is placed in an outer cortical region with venous pooling, whereas the blue arrow is placed medially in a region which likely partial volumes with more microvasculature. **b:** Signal timecourses for both regions. **c,d:** Scatter plots for both regions during room air and carbogen administration, respectively. During both conditions, the lower Z-statistic region exhibits significantly higher variance as quantified by a Bartlett test; room air ($X^2 = 22.0$; $P \leq 0.025$) and carbogen ($X^2 = 20.4$; $P \leq 0.025$). This is consistent with Z-statistic maps being less sensitive to regions of high signal variation, which may arise nonspecifically in draining veins.

Table 1

Patient Demographics and Vascular Information

Case	Age (years)	Sex	Primary stenosed hemisphere	Intracranial vessel (stenosis %)	R PCOM status	L PCOM status
1	35	F	Left	L ICA (92%) L M1 (77%) L A1 (99%)	Present	Fetal-type
2	51	M	Left	L M2 (79%)	Present	Present
3	52	F	Left	L ICA (50%) R M1 (38%)	Absent	Absent
4	47	M	Left	L M1 (80%)	Present	Present
5	45	F	Left	L M1 (72%)	Present	Fetal-type
6	71	F	Left	L ICA(77%) L M2(48%) R M1 (74%)	Absent	Absent
7 (Fig. 2)	46	M	Left	L ICA (93%) L M1 (74%)	Present	Present
8	69	M	Left	L M2 (46%) L A2 (54%)	Present	Fetal-type
9	57	M	Left	L ICA (80%) L M1 (31%) L A1 (50%)	Absent	Present
10	80	M	Left	L ICA (70%)	Present	Present
11	40	F	Right	R M1 (53%)	Present	Present
12	71	F	Right	R M1 (55%)	Absent	Absent

ICA = internal carotid artery; PCOM = posterior communicating artery; M1 = middle cerebral artery (MCA) segment from origin to bifurcation/trifurcation; M2 = MCA segment from bifurcation/trifurcation to origin of cortical branches; A1 = anterior cerebral artery (ACA) segment that originates from the ICA and extends to the anterior communicating (ACOM) artery; A2 = ACA segment that extends from the ACOM to the bifurcation forming the pericallosal and callosomarginal arteries. Note the variability in circle of Willis types (posterior circulation variants only listed here). This suggests that baseline measurements of flow territories may not be sufficient for characterization of tissue-level impairment, but rather full characterization of hemodynamic compensation may require additional measurements of flow territory reactivity.

Table 2

P Values which Reflect Comparison of the Z-Statistics for the Different Flow Labeling Scenarios

	Comparison		
Label scenario	**Affected vs. unaffected**	**Affected vs. VBA**	**Unaffected vs. VBA**
Control	**≤0.002**	**≤0.002**	0.349
Full	**≤0.002**	**≤0.002**	0.669
VBA 1	**≤0.002**	**≤0.002**	0.204
VBA 2	**≤0.002**	**≤0.002**	0.530
R ICA	**≤0.002**	**≤0.002**	0.080
All Conditions	**≤0.002**	**≤0.002**	0.852

VBA = vertebrobasilar. ICA = internal carotid artery. *P*-values represent statistical differences between territories for each labeling scenario. Values in bold represent significant differences ($P \leq 0.002$, Bonferroni corrected). Regardless of labeling scenario, the long-TE BOLD Z-statistics were sensitive to changes between affected and unaffected hemispheres as well as between affected and VBA territories. This is consistent in this population, which had no posterior territory stenosis. As expected, no difference was found when comparing unaffected and VBA regions.